Electronic Supplementary Material (ESI) for Chemical Communications.

Probing the magnetic and magneto-optical properties of a radical-bridged Tb_4 single-molecule magnet

Niki Mavragani,[a] Alexandros A. Kitos,[a] Diogo A. Gálico,[a] Akseli Mansikkamäki[b] and Muralee Murugesu*[a]

Table of Contents

[a] *Department of Chemistry and Biomolecular Sciences, University of Ottawa, 10 Marie Curie, Ottawa, Ontario, K1N 6N5, Canada.*
E-mail: m.murugesu@uottawa.ca
[b] *NMR Research Unit, University of Oulu, P.O. Box 8000, FI-90014, Finland.*

1. Experimental Procedures

General Procedures and Materials: All operations were performed in a Mbraun glovebox under an N_2 atmosphere. Solvents were dried using a J. C. Meyer solvent system, degassed by free-pump-thaw method and stored over activated 4 Å molecular sieves prior to use. The 1,2,4,5-tetrazine (tz) ligand was prepared according to the literature.[1] [Cp*$_2$Tb][(μ-Ph$_2$)BPh$_2$] starting material was prepared according to the literature.[2] All reagents and solvents were purchased from TCI, Alfa Aesar, or Strem Chemicals and used without further purification. HCp* (99+%) was purchased from Alfa Aesar and was degassed/dried as previously described prior to use. The FT-IR sample was prepared under inert conditions between NaCl plates and the spectra recorded on a Nicolet Nexus 550 FT-IR spectrometer in the transmission window of 400-4000 cm^{-1}. Elemental Analysis was performed by Midwest Microlab.

Synthesis of [(Cp*$_2$Tb)$_4$(tz$^{\bullet-}$)$_4$]·3(C$_6$H$_6$) (1): A solution of tz (0.125 mmol, 10 mg) and KC_8 (0.125 mmol, 17mg) in benzene (6 mL) was added to a solution of [Cp*$_2$Tb][(μ-Ph$_2$)BPh$_2$] (0.125 mmol, 93 mg) in benzene (3 mL) to afford a dark red slurry. The mixture was stirred overnight, filtrated, and left undisturbed at room temperature. After several weeks dark red prismatic crystals of **1** suitable for single crystal X-ray were obtained in 32% yield. IR (cm^{-1}): 3034.29 (w), 2970.52 (w), 2899.25 (s), 2855.29 (s), 2721.82 (w), 1827.86 (w), 1529.29 (w), 1478.86 (m), 1427.74 (vs), 1375.81 (m), 1255.21 (m), 1223.89 (vs), 1179.56 (s), 1096.33 (s), 1096.33 (s), 1060.93 (m), 1019.20 (s), 905.98 (m), 891.19(s), 857.32 (w), 804.31 (w), 681.73 (vs), 593.55 (m), 555.20 (w), 535.89 (m), 538.57 (m). Elemental Anal. Calcd: C, 55.84%, H, 6.45%, N, 9.83%, Found: C, 56.07%, H, 6.42%, N, 9.78%.

Single Crystal X-ray Diffraction: Suitable crystals for single-crystal X-ray diffraction (SCXRD) analysis were covered in parabar oil and mounted on a cryoloop. Full data (Table S1) were collected on a Bruker KAPPA APEX-II CCD single-crystal diffractometer (graphite monochromated Mo-Kα radiation, λ = 0.71073 Å), at 203 K temperature. Absorption corrections were applied by using multi-scan of the SADABS[3] program. The structure was solved using direct methods with ShelXT[4] structure solution program and refined by the full-matrix least-squares methods on F^2 with ShelXL[5] refinement package. All non-H atoms were refined by full-matrix least-squares with anisotropic displacement parameters. All H atoms were generated geometrically and were included in the refinement in the riding model approximation. The temperature factors of all H atoms were set to multiple of the equivalent isotropic temperature factors of the parent site (aromatic 1.2 times; methyl 1.5 times the factor). In **1**, there is a positional disorder on all ligands and cocrystallized benzene solvent molecules. After careful refinement, the ratio was found to be close to 50% and the disordered components were left to refine with free variables. Soft restraints were used to handle the disorder groups (SIMU, SADI, ISOR, DFIX etc.). The crystals of **1** consists of non-merohedrally twinned domains (49:51 domain ration) and subsequently, a non-merohedral refinement of the crystal data was employed (see details in the CIF file).

Magnetic Measurements: Magnetic susceptibility measurements for **1** were obtained using a Quantum Design SQUID magnetometer MPMS-XL7 operating between 1.8 and 300 K. Direct current (dc) measurements were performed on crushed polycrystalline sample (8 mg), which was restrained with silicon grease, to avoid possible magnetic-field induced torquing, and sealed in a polyethylene membrane under an inert atmosphere for which diamagnetic corrections were applied. The sample was subjected to dc fields of 70 to -70 kOe while alternating current (ac) measurements took place both in the absence and presence of a static dc field (H_{dc} = 1200 Oe).

Magnetic Circular Dichroism (MCD): MCD measurements were recorded on a Jasco J-1700 CD spectrometer and an Oxford SpectromagPT cryogen-free magneto-optical superconducting magnet system. MCD spectra were recorded on mulls prepared in an inert atmosphere of the solid compound of **1** in Parabar 10312 oil from Hampton Research, sandwiched between quartz slides. The spectrum without any applied field was used as the background for the measurements.

2. Single-crystal X-ray data, molecular features and structural analysis

Table S1. Crystallographic data and refinement details for complex **1**.

Compound reference	1
Chemical formula	$C_{106}H_{146}N_{16}Tb_4$
Formula mass	2280.06
Crystal system	Orthorhombic
a/Å	24.3756(6)
b/Å	20.6384(4)
c/Å	20.7047(4)
α/°	90
β/°	90
γ/°	90
Unit cell volume/Å^3	10416.0(4)
Temperature/K	203(2)
Space group	*C*mca
No. of formula units/unit cell, *Z*	4
F(000)	4616
Theta range for data collection/°	1.624 to 26.999
Index ranges	-31<=h<=31, 0<=k<=26, 0<=l<=26
Radiation type	Mo Kα
Radiation Wavelength/Å	0.71073
Absorption coefficient, *μ*/mm^{-1}	2.735
No. of reflections measured	5816
No. of independent reflections	5816
No. of observed [$I > 2\sigma(I)$] reflections	5203
Data / restraints / parameters	5816 / 889 / 589
Final R_1 values (all data)	0.0757
Final $wR_2(F^2)$ values (all data)	0.1543
Final R_1 values ($I > 2\sigma(I)$)	0.0684
Final $wR_2(F^2)$ values ($I > 2\sigma(I)$)	0.1511
Goodness of fit on F^2	1.367
CCDC number	2271181

Table S2. Selected distances (Å) and angles (º) for complex **1**. Symmetry-related atoms are indicated (').

Distance/angle			Distance/angle
1			
Tb1-Tb2	7.350(7)	Tb1-Tb2'	7.350(7)
Tb1-Tb1'	10.049(7)	Tb2-Tb2'	10.727(7)
Tb2-Tb1-Tb2'	93.75(1)	Tb1-Tb2-Tb1'	86.25(1)
Tb1-N1A	2.510(2)	Tb2-N2A	2.492(2)
Tb1-N3A	2.654(2)	Tb2-N4A	2.714(2)
Tb1-Cp_{cent}*1A	2.394(2)	Tb2-Cp_{cent}*2A	2.420(8)
Tb1-Cp_{cent}*1A'	2.394(2)	Tb2-Cp_{cent}*3A	2.396(8)
Cp_{cent}*1A-Tb1- Cp_{cent}*1A'	139.61(1)	Cp_{cent}*2A-Tb2- Cp_{cent}*3A	136.09(4)
N1A-N3A	1.345(3)	N2-N4A	1.331(3)
N1A-C1A	1.340(3)	N2A-C1A	1.333(3)
N3A-C2A	1.319(3)	N4A-C2A	1.340(2)
N1A-Tb1-N3A	30.02(6)	N2A-Tb2-N4A	29.23(6)
N1A-Tb1-N1A'	77.28(6)	N2A-Tb2-N2A'	74.81(7)
N1A-Tb1-N3A'	107.30(7)	N2A-Tb2-N4A'	104.04(7)
N3A-Tb1-N3A'	137.31(6)	N4A-Tb2-N4A'	133.27(8)
N1A-Tb1- Cp_{cent}*1A	105.71(5)	N2A-Tb2- Cp_{cent}*2A	108.23(5)
N3A-Tb1- Cp_{cent}*1A	97.27(4)	N4A-Tb2- Cp_{cent}*2A	98.88(5)
N1A'-Tb1- Cp_{cent}*1A	105.58(5)	N2A-Tb2- Cp_{cent}*3A	106.31(5)
N3A'-Tb1- Cp_{cent}*1A	97.16(4)	N4A-Tb2- Cp_{cent}*3A	98.17(5)
N2A'-Tb2- Cp_{cent}*2A	108.23(5)	N4A'-Tb2- Cp_{cent}*2A	98.88(5)
N2A'-Tb2- Cp_{cent}*3A	106.31(5)	N4A'-Tb2- Cp_{cent}*3A	98.17(5)

Cp_{cent}*1A: C3A-C12A, Cp_{cent}*2A: C13A-C18A, Cp_{cent}*3A: C19A-C24A

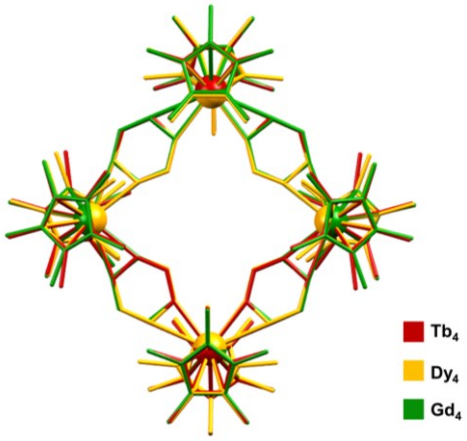

Fig. S1: Structural overlay of "**Tb_4**" (dark red), "**Dy_4**" (orange) and "**Gd_4**" (green), highlighting that all complexes are isostructural. H-atoms, benzene lattice solvent molecules and disorder conformers have been omitted for clarity.

Table S3. Comparison of the unit cell parameters of **$[(Cp^*_2Dy)_4(tz^{\bullet-})_4]\cdot 3(C_6H_6)$**, **$[(Cp^*_2Gd)_4(tz^{\bullet-})_4]\cdot 3(C_6H_6)$** and **$[(Cp^*_2Tb)_4(tz^{\bullet-})_4]\cdot 3(C_6H_6)$**.

Compound	a/Å	*b*/Å	*c*/Å	*α*/°	*β*/°	*γ*/°	V/Å^3	Space group	Reference
$[(Cp^*_2Dy)_4(tz^{\bullet-})_4]\cdot 3(C_6H_6)$	24.1465(9)	20.4504(8)	20.4513(8)	90	90	90	10099.0(7)	*Cmca*	13
$[(Cp^*_2Gd)_4(tz^{\bullet-})_4]\cdot 3(C_6H_6)$	24.396(2)	20.6895(18)	20.7047(18)	90	90	90	10450.6(16)	*Cmca*	13
$[(Cp^*_2Tb)_4(tz^{\bullet-})_4]\cdot 3(C_6H_6)$	24.3756(6)	20.6384(4)	20.7047(4)	90	90	90	10416.0(4)	*Cmca*	This work

Structural analysis of 1:

The centrosymmetric molecular structure of **1** (Fig. 1B and S2) consists of four $[Cp^*_2Tb^{III}]^+$ moieties bridged by four μ-$tz^{\bullet-}$ ligands forming a diamond-like core, where all four Tb^{III} metal ions lie on the same plane (Fig. 1B). The average Tb-Cp^*_{cent} bond distance is 2.401(4) Å, which is similar to the respective distance observed in the $tz^{\bullet-}$-bridged $[(Cp^*_2Tb)_2(tz^{\bullet-})(THF)]BPh_4$ (THF = tetrahydrofuran) "**Tb_2**" complex (2.405(5) Å), while the respective Cp^*_{cent}-Tb-Cp^*_{cent} angle is found to be slightly increased (**1**: 137.85(4)°; "**Tb_2**" dimer; 136.4(2)°).[6] The Tb−N bond distances (av. 2.582(2) Å for Tb1 and av. 2.603(2) Å for Tb2) are similar to those observed for the "**Ln_4**" (average bond distance: Dy-N_{tz}: 2.585(2) Å; Gd-N_{tz}: 2.618(2) Å), as expected, although slightly longer than the respective distance on the "**Tb_2**"; 2.469(2) Å. The radical nature of the tetrazine ring is corroborated by the clear elongation of N···N bond distances (1.345(3) Å and 1.331(3) Å) compared to the neutral free ligand (1.327(6) Å).[7] In the "**Tb_4**" core, the shortest intramolecular Tb···Tb distance is 7.350(7) Å, while the longest distance separating the diagonals is found to be 10.727(7) Å (Fig. S3). The packing arrangement reveals that the "**Tb_4**" units are in relatively close proximity (Fig. S4), where the intermolecular Tb···Tb distances vary between 10.340(10) Å and 10.754(12) Å (Fig. S5). These values are in the same range as the largest intramolecular Tb···Tb distance of 10.727(7) Å.

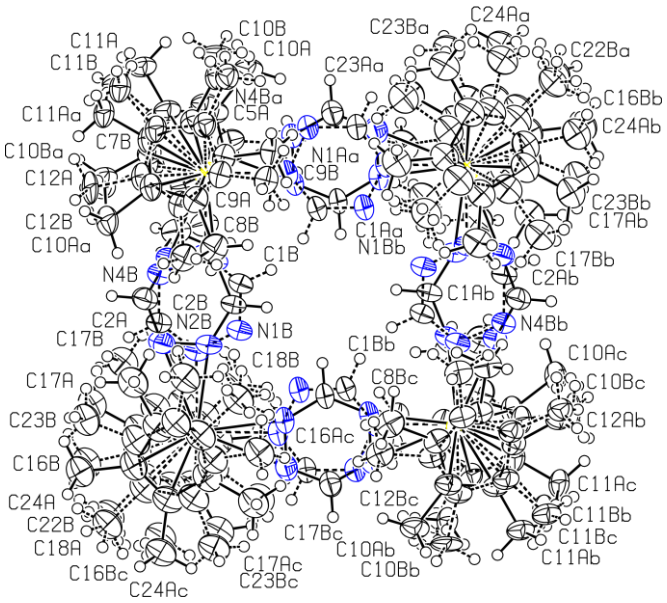

Fig. S2: ORTEP diagram of **1**. Displacement ellipsoids are drawn at the 50% probability level. Symmetry codes: (*a*) *x*, 1 − *y*, 1 − *z*; (*b*) 1 − *x*, 1 − *y*, 1 − *z*; (*c*) 1 − *x*, *y*, *z*. The benzene solvent molecules have been omitted for clarity.

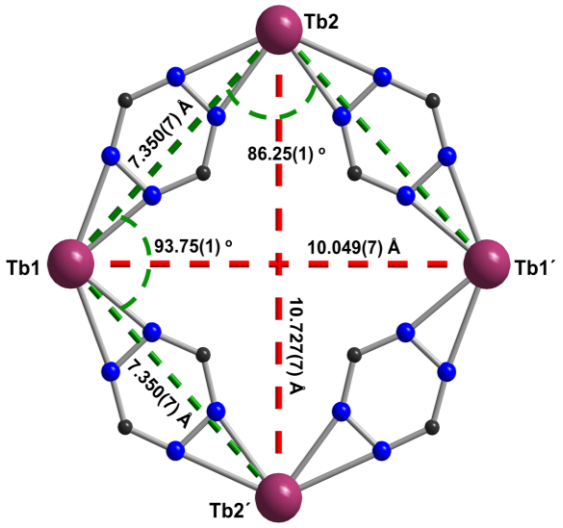

Fig. S3: Molecular structure of **1** highlighting the intramolecular Tb···Tb distances and angles of the diamond-like core. Cp*, H-atoms, disorder conformers and lattice solvent molecules have been omitted for clarity.

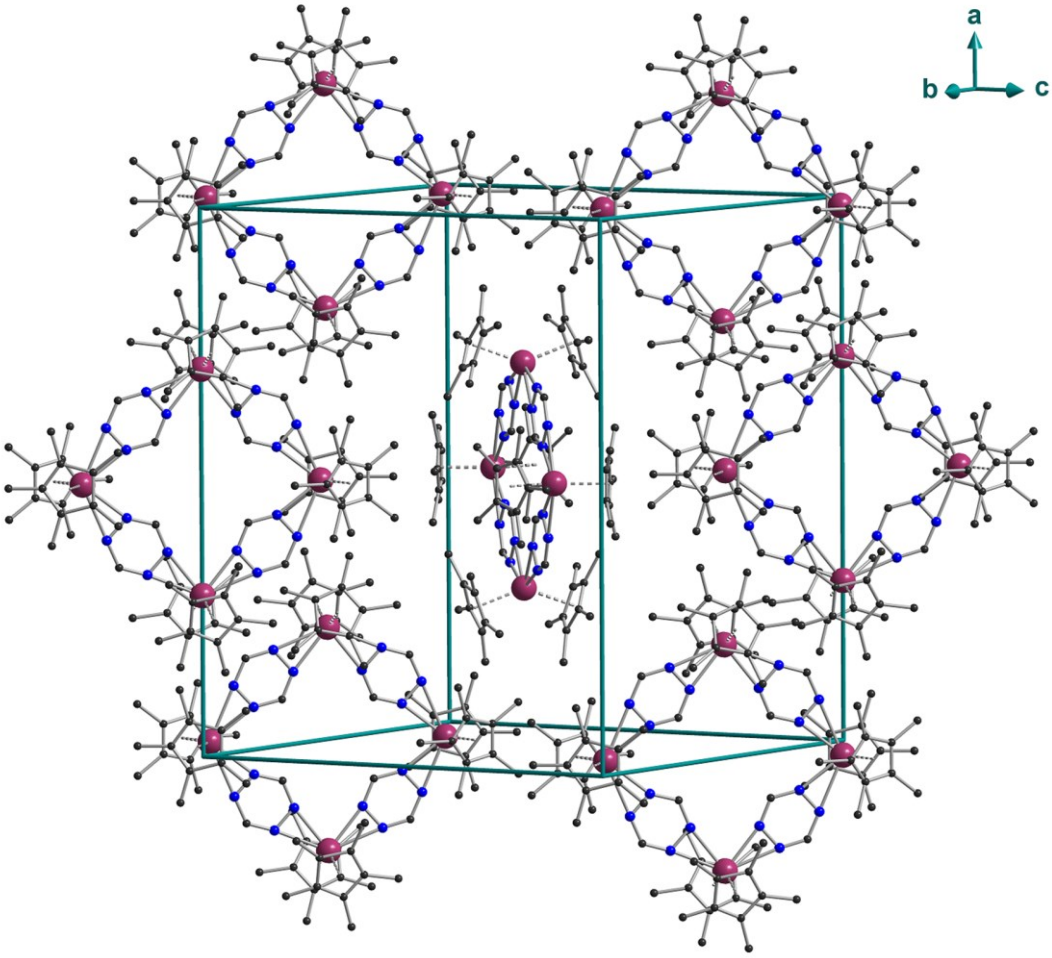

Fig. S4: Molecular packing of **1**. Lattice solvent molecules, H-atoms and disorder conformers have been omitted for clarity. Colour code: Tb (purple), C (grey), and N (blue).

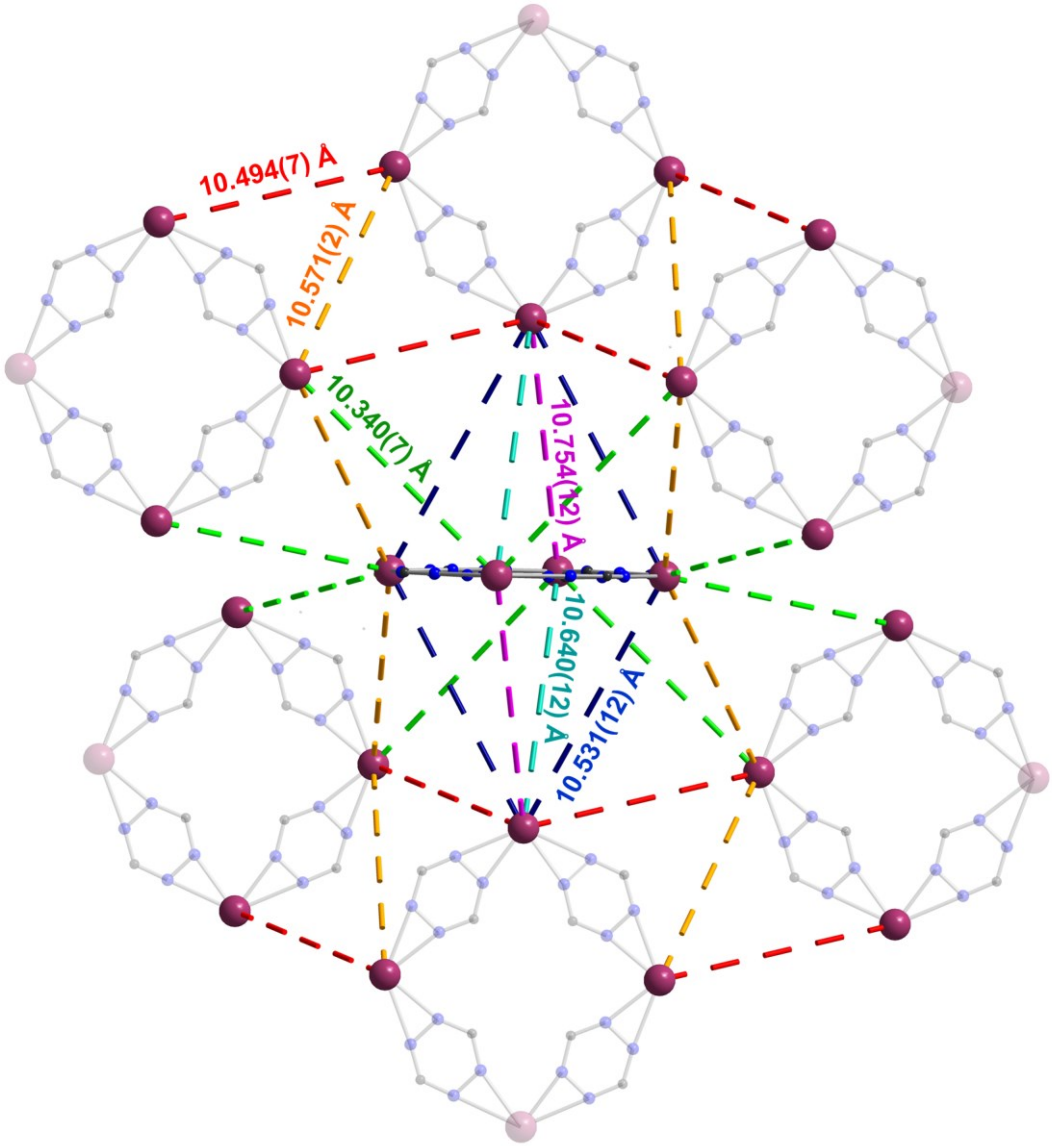

Fig. S5: Intermolecular Tb···Tb distances. For clarity reasons, partial transparency has been employed and Cp* as well as H-atoms and lattice solvent molecules have been omitted. Each Tb···Tb distance is colour coded.

3. Additional magnetic data

Dc Magnetism Plots:

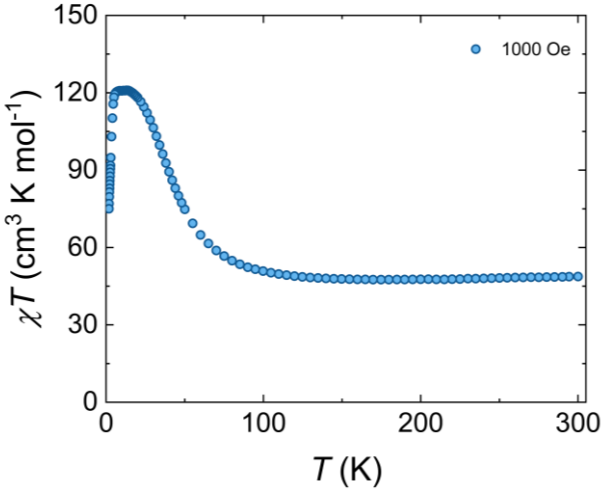

Fig. S6: Variable temperature χT *vs.* T plot of **1** under an applied static dc field of 1000 Oe.

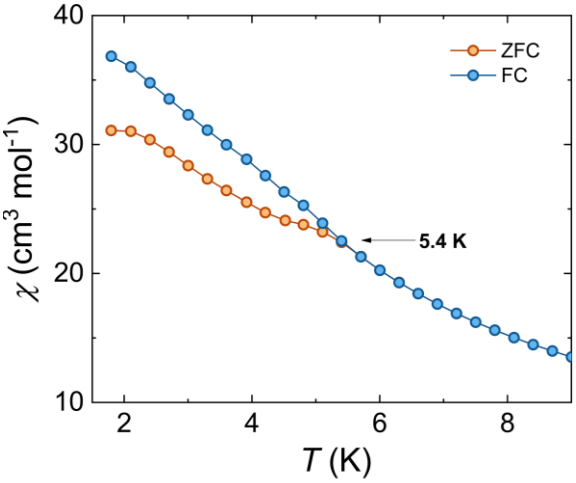

Fig. S7: Zero-field-cooled and field-cooled (ZFC/FC) curves for **1** under an applied static field of 1000 Oe. Data were collected at an average sweep rate of 0.3 K min^{-1}. ZFC and FC susceptibilities bifurcate at 5.4 K, as indicated by the respective black arrows.

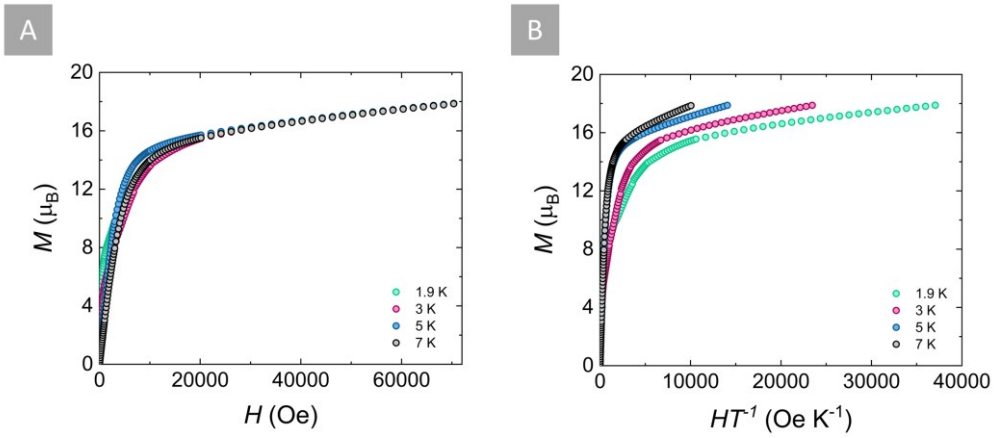

Fig. S8: Field-dependence plots of the magnetization and the reduced magnetization for **1** collected between 0 and 70 kOe at the respective temperature ranges with an average sweep rate of 15 Oe/s.

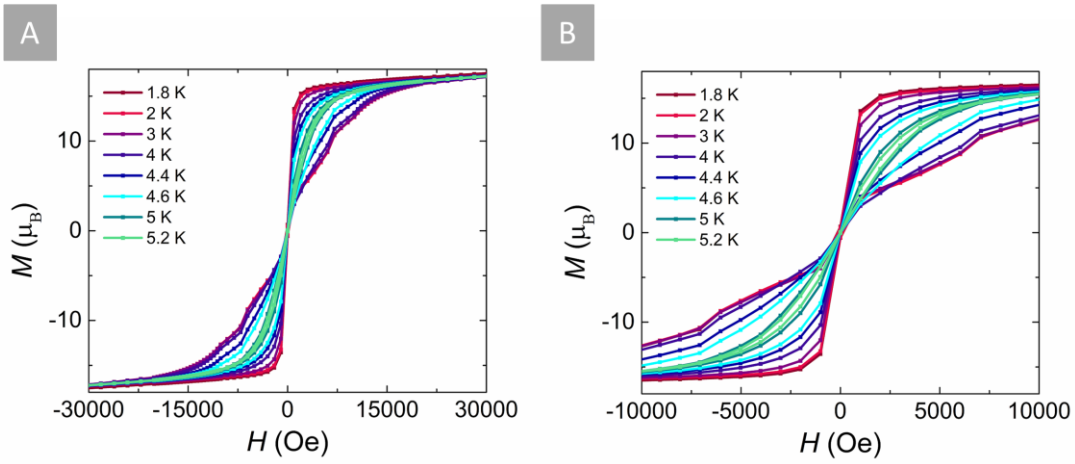

Fig. S9: (A) Magnetic hysteresis data for **1** in the respective temperature region collected with an average sweep rate of 25 Oe/s. (B) Zoomed-in area of the hysteresis loop at the indicated temperature region.

Ac Magnetism Plots:

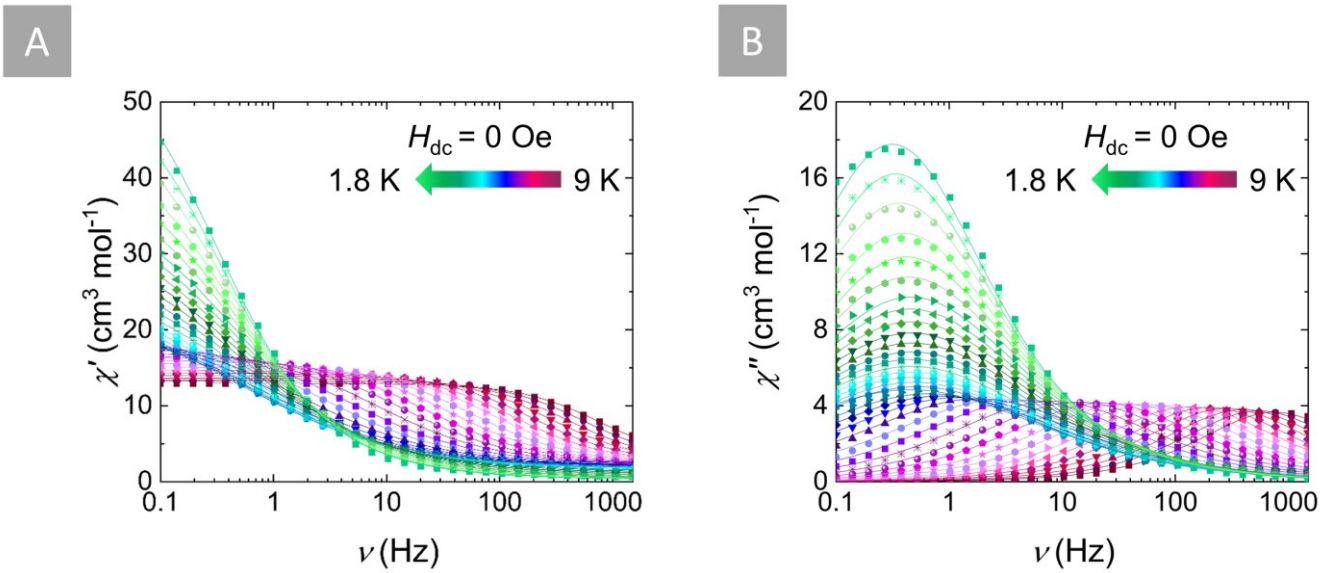

Fig. S10: Frequency-dependence of χ' (A) and χ'' (B) as a function of temperature in the 9 to 1.8 K temperature range, in the absence of an applied field (H_{dc} = 0 Oe) for **1**. Solid lines represent best fits to the generalized Debye model.

Table S4. Fitting parameters obtained from CCFit-2[8] using a generalized Debye model for the ac data of **1** in the absence of a static dc field (H_{dc} = 0 Oe) in the temperature region of 1.8 to 9 K (Fig. 2A, S10).

T (K)	τ (s)	α	χ_s (cm^3 mol^{-1})	χ_t (cm^3 mol^{-1})
1.8	5.08 x 10^{-1}	3.32 x 10^{-1}	2.97 x 10^{-1}	61.7
2	4.74 x 10^{-1}	3.41 x 10^{-1}	2.92 x 10^{-1}	57.2
2.2	4.39 x 10^{-1}	3.51 x 10^{-1}	2.80 x 10^{-1}	52.8
2.4	4.04 x 10^{-1}	3.66 x 10^{-1}	2.96 x 10^{-1}	48.5
2.6	3.81 x 10^{-1}	3.82 x 10^{-1}	3.27 x 10^{-1}	45.2
2.8	3.65 x 10^{-1}	3.98 x 10^{-1}	3.88 x 10^{-1}	42.5
3	3.47 x 10^{-1}	4.15 x 10^{-1}	4.42 x 10^{-1}	39.7
3.2	3.51 x 10^{-1}	4.27 x 10^{-1}	5.77 x 10^{-1}	38.2
3.4	3.46 x 10^{-1}	4.36 x 10^{-1}	7.21 x 10^{-1}	36.2
3.6	3.42 x 10^{-1}	4.44 x 10^{-1}	8.65 x 10^{-1}	34.4
3.8	3.39 x 10^{-1}	4.49 x 10^{-1}	1.02	32.7
4	3.41 x 10^{-1}	4.54 x 10^{-1}	1.16	31.1
4.2	3.41 x 10^{-1}	4.57 x 10^{-1}	1.28	29.7
4.4	3.44 x 10^{-1}	4.61 x 10^{-1}	1.40	28.4
4.6	3.44 x 10^{-1}	4.62 x 10^{-1}	1.53	27.2
4.8	3.38 x 10^{-1}	4.61 x 10^{-1}	1.63	26.0
5	3.25 x 10^{-1}	4.60 x 10^{-1}	1.72	25.0
5.2	3.05 x 10^{-1}	4.59 x 10^{-1}	1.79	23.9
5.4	3.53 x 10^{-1}	4.90 x 10^{-1}	1.72	24.6
5.6	2.40 x 10^{-1}	4.60 x 10^{-1}	1.89	22.4
5.8	1.9 x 10^{-1}	4.54 x 10^{-1}	1.93	21.7
6	1.36 x 10^{-1}	4.43 x 10^{-1}	1.98	20.9
6.2	8.88 x 10^{-2}	4.26 x 10^{-1}	2.04	20.1
6.4	5.47 x 10^{-2}	4.07 x 10^{-1}	2.07	19.3
6.6	3.26 x 10^{-2}	3.88 x 10^{-1}	2.10	18.5
6.8	1.94 x 10^{-2}	3.70 x 10^{-1}	2.13	17.8
7	1.16 x 10^{-2}	3.51 x 10^{-1}	2.17	17.2
7.2	7.03 x 10^{-3}	3.36 x 10^{-1}	2.18	16.6
7.4	4.38 x 10^{-3}	3.18 x 10^{-1}	2.22	16.1
7.6	2.77 x 10^{-3}	3.06 x 10^{-1}	2.22	15.6
7.8	1.80 x 10^{-3}	2.89 x 10^{-1}	2.28	15.1
8	1.19 x 10^{-3}	2.79 x 10^{-1}	2.29	14.7
8.2	8.06 x 10^{-4}	2.63 x 10^{-1}	2.35	14.3
8.4	5.55 x 10^{-4}	2.50 x 10^{-1}	2.41	13.9
8.6	3.96 x 10^{-4}	2.34 x 10^{-1}	2.56	13.6
8.8	2.88 x 10^{-4}	2.18 x 10^{-1}	2.71	13.3
9	2.11 x 10^{-4}	2.04 x 10^{-1}	2.85	13.0

Fit of the temperature- and field-dependent relaxation times for 1:

To further investigate the relaxation dynamics in **1**, the extracted relaxation times from the temperature-dependent ac susceptibility (χ' and χ'') when H_{dc} = 0 Oe, can be fit to the following equation (S1):

$$\tau^{-1} = \tau_{QTM}^{-1} + \tau_0^{-1}\exp(-U_{eff}/k_BT) \text{ (S1).}$$

where a combination of QTM and Orbach processes provided the following best-fit parameters: τ_{QTM} = 0.41 s, τ_0 = 1.67 x 10^{-10} s and U_{eff} = 87.8 cm^{-1}. For the field-dependent relaxation times, an excellent fit of the τ was achieved by using equation (S2):

$$\tau^{-1} = (B_1/1+B_2H_2) + \tau_0^{-1}\exp(-U_{eff}/k_BT) \text{ (S2)}$$

yielding the following best-fit parameters: B_1 = 0.25 s, B_2 = 1.94 x 10^{-5} Oe^{-2}, τ_0 = 1.84 x 10^{-10} s and U_{eff} = 88.0 cm^{-1}. Lastly, the extracted relaxation times from the temperature-dependent ac susceptibility (χ' and χ'') when H_{dc} = 1200 Oe, can be fit to the following equation (S3):

$$\tau^{-1} = \tau_0^{-1}\exp(-U_{eff}/k_BT) \text{ (S3)}$$

with the following best-fit parameters: τ_0 = 1.27 x 10^{-10} s and U_{eff} = 89.4 cm^{-1}.

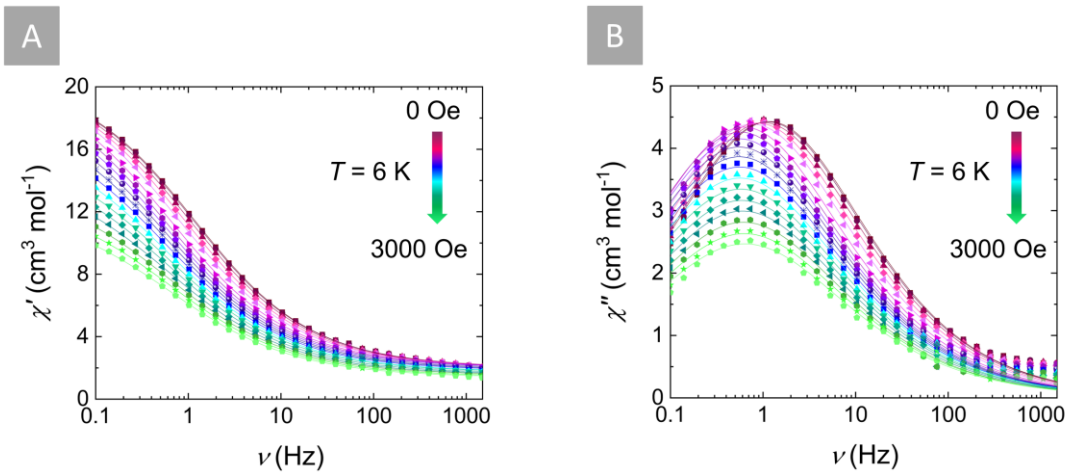

Fig. S11: Field-dependence of the χ' (A) and χ'' (B) magnetic susceptibility of **1** at 6 K in the field range of 0 to 5000 Oe. The solid lines represent the best fit to the generalized Debye model.

Table S5. Best-fit parameters to the generalized Debye model for the frequency dependence of the out-of-phase-magnetic susceptibility (χ'') as a function of field for **1** collected at T = 6 K (Figure S11).

H (Oe)	τ (s)	α	χ_s (cm^3 mol^{-1})	χ_t (cm^3 mol^{-1})
0	1.36 x 10^{-1}	4.43 x 10^{-1}	1.98	20.9
100	1.42 x 10^{-1}	4.44 x 10^{-1}	2.00	21.0
200	1.57 x 10^{-1}	4.47 x 10^{-1}	1.99	21.0
300	1.80 x 10^{-1}	4.49 x 10^{-1}	2.00	21.1
400	2.08 x 10^{-1}	4.52 x 10^{-1}	2.02	21.1
600	2.56 x 10^{-1}	4.55 x 10^{-1}	2.03	21.1
800	2.87 x 10^{-1}	4.54 x 10^{-1}	1.99	20.2
1000	2.80 x 10^{-1}	4.55 x 10^{-1}	2.02	20.7
1200	2.88 x 10^{-1}	4.55 x 10^{-1}	1.93	19.6
1400	2.87 x 10^{-1}	4.57 x 10^{-1}	1.87	18.9
1600	2.85 x 10^{-1}	4.58 x 10^{-1}	1.83	18.1
1800	2.82 x 10^{-1}	4.61 x 10^{-1}	1.74	17.4
2000	2.78 x 10^{-1}	4.60 x 10^{-1}	1.71	16.5
2200	2.72 x 10^{-1}	4.61 x 10^{-1}	1.63	15.7
2400	2.65 x 10^{-1}	4.59 x 10^{-1}	1.57	14.8
2600	2.60 x 10^{-1}	4.58 x 10^{-1}	1.53	14.0
2800	2.54 x 10^{-1}	4.63 x 10^{-1}	1.44	13.2
3000	2.51 x 10^{-1}	4.65 x 10^{-1}	1.38	12.4

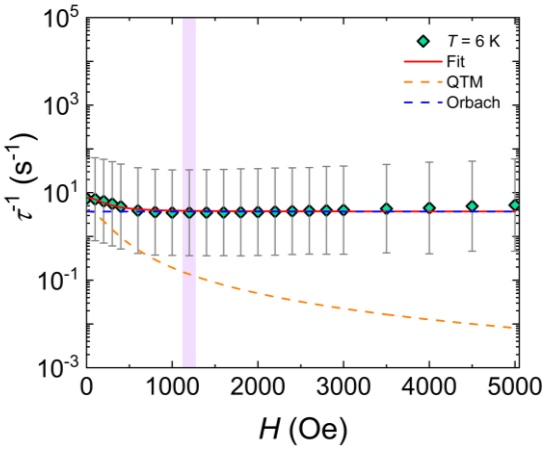

Fig. S12: Field-dependence of the relaxation times (τ^{-1}) for **1** at a fixed temperature of 6 K with the respective estimated standard deviations (gray bars). The estimated standard deviations of the τ were estimated from the α-parameters of the generalized Debye fits and the log-normal distribution as described in ref. 8. The relaxation times were obtained from the generalized Debye model (*see*, Table S4). The optimal static field for which the relaxation times are longest and quantum tunneling of the magnetization is suppressed, is highlighted with a light-pink line. This is the field at which temperature-dependent relaxation studies under a static dc field were completed at (*vide infra*). The solid red lines represent the best-fit based on eqn. (S2), while the dashed orange and blue lines in represent the individual components of the magnetic relaxation for QTM and Orbach process, respectively.

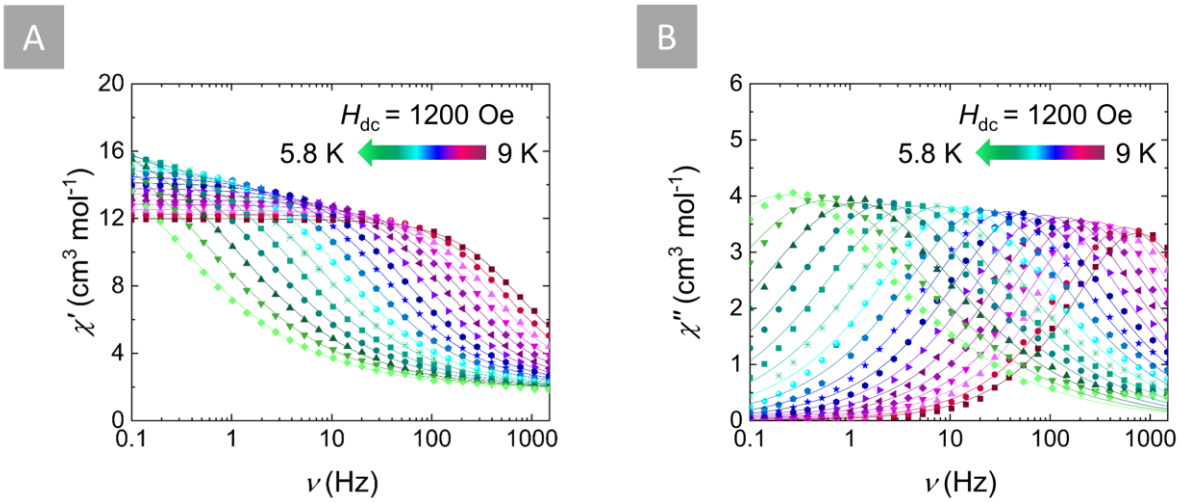

Fig. S13: Frequency-dependence of χ' (A) and χ'' (B) as a function of temperature in the 9 to 5.8 K temperature range, under an applied static field of 1200 Oe for **1**. Solid lines represent best fits to the generalized Debye model.

Table S6. Fitting parameters obtained from CCFit-2[8] using a generalized Debye model for the ac data of **1** in the presence of a static dc field (H_{dc} = 1200 Oe) in the temperature region of 5.8 to 9 K (Fig. 5C, S13).

T (K)	τ (s)	α	χ_s (cm^3 mol^{-1})	χ_t(cm^3 mol^{-1})
5.8	7.17 x 10^{-1}	4.88 x 10^{-1}	1.85	20.7
6	2.93 x 10^{-1}	4.57 x 10^{-1}	1.89	19.1
6.2	1.36 x 10^{-1}	4.28 x 10^{-1}	1.91	18.0
6.4	6.95 x 10^{-2}	4.07 x 10^{-1}	1.94	17.3
6.6	3.70 x 10^{-2}	3.86 x 10^{-1}	1.96	16.6
6.8	2.05 x 10^{-2}	3.62 x 10^{-1}	2.00	15.9
7	1.18 x 10^{-2}	3.47 x 10^{-1}	1.98	15.5
7.2	7.12 x 10^{-3}	3.35 x 10^{-1}	2.00	15.0
7.4	4.32 x 10^{-3}	3.19 x 10^{-1}	2.02	14.6
7.6	2.76 x 10^{-3}	3.02 x 10^{-1}	2.09	14.2
7.8	1.76 x 10^{-3}	2.91 x 10^{-1}	2.08	13.8
8	1.17 x 10^{-3}	2.76 x 10^{-1}	2.13	13.5
8.2	7.98 x 10^{-4}	2.63 x 10^{-1}	2.20	13.2
8.4	5.58 x 10^{-4}	2.45 x 10^{-1}	2.31	12.8
8.6	3.93 x 10^{-4}	2.35 x 10^{-1}	2.38	12.5
8.8	2.83 x 10^{-4}	2.15 x 10^{-1}	2.55	12.3
9	2.15 x 10^{-4}	1.98 x 10^{-1}	2.83	12.0

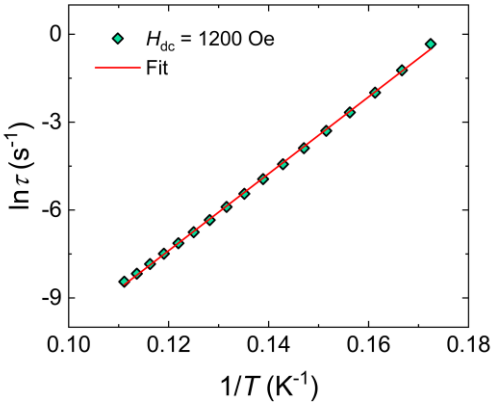

Fig. S14: Arrhenius plot of the natural log of the relaxation time, τ, of the magnetization for **1** (teal diamonds) versus the inverse temperature. The red line represents the linear fit to the Arrhenius equation that affords a U_{eff} = 91.2 cm^{-1}.

4. Computational details

Complex **1** consists of four Tb^{III} ions, two of which are crystallographically independent. These will be labeled according to their crystal structure labels Tb1 and Tb2. The geometry of **1** was extracted from the crystal structure and non-coordinated solvent molecules were removed from the structure. The positions of hydrogen atoms were optimized using density functional theory while the positions of heavier atoms were kept frozen to their crystal-structure coordinates. The geometry optimization was carried out using the *Gaussian16* software revision C.02[9] and the pure GGA exchange-correlation (XC) functional PBE.[10] The Tb^{III} ions were treated using the 4*f*-in-core Stuttgart pseudopotential MWB54 along with a corresponding valence basis set.[11] The remaining atoms were treated using polarized double-ζ quality def2-SVP basis sets.[12]

The local properties of each Tb^{III} ion were calculated using the crystal-field averaging procedure described in our earlier work.[13] In this approach, only a single Tb^{III} ion was considered in a given calculation. The remaining three Tb^{III} ions in the structure were replaced by diamagnetic Y^{III} ions. The paramagnetic radical ligands were introduced into the crystal-field in an average manner: first a calculation was carried out where the unpaired electron was removed from the ligands, then another calculation was carried out where an extra electron was added on the radical ligands. In both cases, the radical ligands are diamagnetic. The *ab initio* crystal-field parameters[14] were extracted from both calculations, and the crystal-field of the radical system was calculated as the arithmetic average of the two crystal fields. The crystal-field operator is then diagonalized to yield the final eigenstates and eigenvalues. This introduces an approximation that is justified when the effect of the unpaired electron on the Tb^{III} ions is weak and primarily of electrostatic nature. Since lanthanides rarely display strong exchange interaction, this approximation should be well justified. The *ab initio* crystal-field parameters along with the average parameters are listed in Tables S7 and S8.

A total of four different systems needs to be calculated: the two systems with one electron removed and one electron added for both Tb1 and Tb2. In each case state-averaged complete active space self-consistent field (SA-CASSCF) type multireference calculations were carried out.[15] The calculations were conducted using the *Orca* code version 5.0.4.[16] The active space consisted of the seven 4*f* orbitals and eight 4*f*-electrons. All seven septet and 140 pentet states were solved in a single SA-CASSCF calculation for each of the four systems. Electron correlation effects outside the active space were estimated using the second-order *N*-electron valence state perturbation theory (NEVPT2) in its strongly contracted formulation.[17] To reduce the computational costs, a single set of orbitals were used for all states in the NEVPT2 procedure.

Scalar relativistic effects were treated in the multireference calculations using the standard second-order Douglas–Kroll–Heß (DKH) transformation.[18] Spin-orbit coupling (SOC) was introduced using the well-established quasi-degenerate perturbation theory (QDPT) approach,[19] where the spin-orbit coupled Hamiltonian is constructed in a basis of the SA-CASSCF eigenstates and diagonalized to yield the final spin-orbit coupled eigenstates and eigenvalues. The SOC operator was constructed using the spin-orbit mean-field (SOMF) approximation.[20] Polarized triple-ζ quality SARC-DKH-TZVP basis sets[21,22] were used for the Tb^{III} and Y^{III} ions, and double-ζ quality DKH-def2-SV(P) basis sets[12,22] with valence-polarization functions for non-hydrogen atoms were used for the remaining atoms. The auxiliary basis sets used in the integral transformation were generated using the "AutoAux" feature in *Orca*.[23] The ***g*** tensors of the quasidoublets were calculated following the well-established methodology.[24] The construction of the crystal-field operators and the calculation of the ***g*** tensors was carried out using our own code. In the calculation, the magnetic moments were calculated using the full crystal-field eigenstates and the *LS* coupling approximation for the construction of the magnetic moment operators.

Similarly to the "**Dy_4**", the principal magnetic axes of all ions in **1** are almost collinear (Fig. S15). The axes are perpendicular to the molecular plane, clearly showing that the strong axiality of the CF arising from the Cp* ligands is stronger than the equatorial contribution to the CF arising from the bridging $tz^{\bullet-}$ ligands.

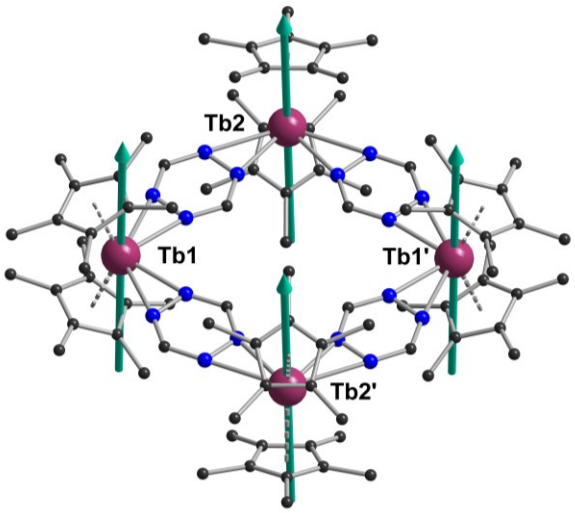

Fig. S15: Orientation of the *ab initio* calculated principal magnetic axes (teal vectors) for **1**.

Table S7. *Ab initio* crystal-field parameters following the Iwahara–Chibotaru[25] notation (in units cm^{-1}) calculated for Tb1 ions.

		One electron removed			One electron added			Average		
k	***q*** [a]	**Re(B_{kq})**	**Im(B_{kq})**	**$\|B_{kq}\|$**	**Re(B_{kq})**	**Im(B_{kq})**	**$\|B_{kq}\|$**	**Re(B_{kq})**	**Im(B_{kq})**	**$\|B_{kq}\|$**
2	0	–528.274	0.000	528.274	–72.816	0.000	72.816	–300.545	0.000	300.545
2	1	1.337	–0.016	1.337	–0.056	–0.002	0.056	0.640	–0.009	0.640
2	2	47.858	–1.058	47.870	40.308	–7.343	40.971	44.083	–4.200	44.283
4	0	80.092	0.000	80.092	21.144	0.000	21.144	50.618	0.000	50.618
4	1	–1.609	0.019	1.609	0.022	–0.003	0.023	–0.793	0.008	0.793
4	2	–0.308	0.005	0.308	6.773	2.454	7.204	3.233	1.230	3.459
4	3	3.743	–0.123	3.745	–0.029	–0.003	0.030	1.857	–0.063	1.858
4	4	13.177	–0.584	13.190	43.033	1.879	43.074	28.105	0.647	28.113
6	0	–1.464	0.000	1.464	10.911	0.000	10.911	4.724	0.000	4.724
6	1	0.707	–0.008	0.707	0.026	–0.002	0.026	0.367	–0.005	0.367
6	2	–4.807	0.105	4.808	–2.002	0.412	2.044	–3.404	0.258	3.414
6	3	–0.854	0.028	0.855	–0.010	–0.003	0.010	–0.432	0.013	0.432
6	4	–0.705	0.031	0.705	3.853	1.640	4.187	1.574	0.836	1.782
6	5	0.270	–0.015	0.270	–0.003	–0.003	0.004	0.133	–0.009	0.133
6	6	–9.131	0.605	9.151	8.133	4.198	9.152	–0.499	2.402	2.453
8	0	–0.065	0.000	0.065	–0.196	0.000	0.196	–0.130	0.000	0.130
8	1	–0.089	0.001	0.089	–0.001	0.000	0.001	–0.045	0.001	0.045
8	2	0.639	–0.013	0.640	0.101	–0.003	0.101	0.370	–0.008	0.370
8	3	0.089	–0.003	0.089	0.000	0.000	0.000	0.044	–0.001	0.044
8	4	–0.025	0.001	0.025	0.069	0.010	0.070	0.022	0.005	0.023

8	5	–0.023	0.001	0.023	0.001	0.000	0.001	–0.011	0.001	0.011
8	6	0.262	–0.017	0.263	–0.081	–0.047	0.094	0.090	–0.032	0.096
8	7	0.010	–0.001	0.010	0.000	0.000	0.000	0.005	0.000	0.005
8	8	–0.081	0.007	0.081	0.190	0.033	0.193	0.055	0.020	0.058
10	0	0.013	0.000	0.013	0.004	0.000	0.004	0.008	0.000	0.008
10	1	0.005	0.000	0.005	0.000	0.000	0.000	0.002	0.000	0.002
10	2	–0.041	0.001	0.041	0.001	0.000	0.001	–0.020	0.000	0.020
10	3	–0.004	0.000	0.004	0.000	0.000	0.000	–0.002	0.000	0.002
10	4	0.004	0.000	0.004	0.006	0.002	0.007	0.005	0.001	0.005
10	5	0.001	0.000	0.001	0.000	0.000	0.000	0.001	0.000	0.001
10	6	–0.002	0.000	0.002	0.011	0.006	0.013	0.005	0.003	0.006
10	7	0.000	0.000	0.000	0.000	0.000	0.000	0.000	0.000	0.000
10	8	0.004	0.000	0.004	0.001	0.000	0.001	0.003	0.000	0.003
10	9	0.000	0.000	0.000	0.000	0.000	0.000	0.000	0.000	0.000
10	10	–0.002	0.000	0.002	0.013	0.009	0.016	0.005	0.005	0.007
12	0	0.000	0.000	0.000	0.000	0.000	0.000	0.000	0.000	0.000
12	1	0.000	0.000	0.000	0.000	0.000	0.000	0.000	0.000	0.000
12	2	0.000	0.000	0.000	0.000	0.000	0.000	0.000	0.000	0.000
12	3	0.000	0.000	0.000	0.000	0.000	0.000	0.000	0.000	0.000
12	4	0.000	0.000	0.000	0.000	0.000	0.000	0.000	0.000	0.000
12	5	0.000	0.000	0.000	0.000	0.000	0.000	0.000	0.000	0.000
12	6	0.000	0.000	0.000	0.000	0.000	0.000	0.000	0.000	0.000
12	7	0.000	0.000	0.000	0.000	0.000	0.000	0.000	0.000	0.000
12	8	0.000	0.000	0.000	0.000	0.000	0.000	0.000	0.000	0.000
12	9	0.000	0.000	0.000	0.000	0.000	0.000	0.000	0.000	0.000
12	10	0.000	0.000	0.000	0.000	0.000	0.000	0.000	0.000	0.000
12	11	0.000	0.000	0.000	0.000	0.000	0.000	0.000	0.000	0.000
12	12	0.000	0.000	0.000	0.000	0.000	0.000	0.000	0.000	0.000

[a] The CF parameters are only listed for non-negative values of q. The values with negative q are given by $B_{k-q} = (-1)^q B_{kq}^*$.

Table S8. *Ab initio* crystal-field parameters following the Iwahara–Chibotaru[25] notation (in units cm^{-1}) calculated for Tb2 ions.

		One electron removed			One electron added			Average		
k	***q*** [a]	**Re(B_{kq})**	**Im(B_{kq})**	**$\lvert B_{kq}\rvert$**	**Re(B_{kq})**	**Im(B_{kq})**	**$\lvert B_{kq}\rvert$**	**Re(B_{kq})**	**Im(B_{kq})**	**$\lvert B_{kq}\rvert$**
2	0	–455.063	0.000	455.063	–169.633	0.000	169.633	–312.348	0.000	312.348
2	1	3.002	–0.153	3.006	–73.966	3.112	74.031	–35.482	1.479	35.513
2	2	–47.648	3.371	47.767	78.016	–7.088	78.337	15.184	–1.858	15.297
4	0	66.922	0.000	66.922	13.829	0.000	13.829	40.376	0.000	40.376

4	1	–2.336	0.124	2.339	19.516	–0.767	19.531	8.590	–0.322	8.596
4	2	–5.694	0.439	5.711	7.601	–0.674	7.631	0.954	–0.117	0.961
4	3	2.267	–0.248	2.281	–14.796	2.110	14.946	–6.264	0.931	6.333
4	4	8.779	–1.314	8.876	30.595	–5.535	31.092	19.687	–3.425	19.982
6	0	–1.201	0.000	1.201	2.999	0.000	2.999	0.899	0.000	0.899
6	1	0.708	–0.038	0.709	6.091	–0.234	6.096	3.399	–0.136	3.402
6	2	5.331	–0.406	5.346	3.722	–0.299	3.734	4.526	–0.353	4.540
6	3	–0.872	0.098	0.878	–2.517	0.384	2.546	–1.694	0.241	1.712
6	4	0.238	–0.035	0.241	3.938	–0.732	4.006	2.088	–0.384	2.123
6	5	–0.041	0.007	0.042	–0.390	0.138	0.414	–0.216	0.073	0.228
6	6	9.205	–2.066	9.434	7.153	–1.952	7.415	8.179	–2.009	8.422
8	0	–0.025	0.000	0.025	0.380	0.000	0.380	0.177	0.000	0.177
8	1	–0.086	0.004	0.087	–0.426	0.021	0.427	–0.256	0.013	0.257
8	2	–0.606	0.048	0.608	–0.163	0.011	0.163	–0.384	0.029	0.385
8	3	0.081	–0.009	0.082	–0.041	0.003	0.041	0.020	–0.003	0.020
8	4	–0.094	0.014	0.096	–0.103	0.019	0.105	–0.099	0.017	0.100
8	5	0.020	–0.004	0.020	0.080	–0.019	0.082	0.050	–0.011	0.051
8	6	–0.239	0.055	0.245	–0.018	0.004	0.018	–0.128	0.030	0.132
8	7	0.000	0.000	0.000	–0.052	0.018	0.055	–0.026	0.009	0.027
8	8	–0.093	0.028	0.097	0.144	–0.054	0.154	0.026	–0.013	0.029
10	0	0.005	0.000	0.005	–0.023	0.000	0.023	–0.009	0.000	0.009
10	1	0.007	0.000	0.007	0.004	0.000	0.004	0.005	0.000	0.005
10	2	0.034	–0.003	0.034	0.012	–0.001	0.012	0.023	–0.002	0.023
10	3	–0.004	0.000	0.004	–0.005	0.001	0.005	–0.004	0.001	0.005
10	4	0.006	–0.001	0.006	0.008	–0.002	0.008	0.007	–0.001	0.007
10	5	–0.002	0.000	0.002	–0.010	0.002	0.010	–0.006	0.001	0.006
10	6	0.002	–0.001	0.002	0.002	–0.001	0.002	0.002	–0.001	0.002
10	7	0.000	0.000	0.000	–0.001	0.000	0.001	0.000	0.000	0.000
10	8	0.004	–0.001	0.005	0.003	–0.001	0.003	0.004	–0.001	0.004
10	9	0.000	0.000	0.000	–0.004	0.002	0.004	–0.002	0.001	0.002
10	10	0.002	–0.001	0.003	0.009	–0.004	0.010	0.006	–0.003	0.006
12	0	0.000	0.000	0.000	0.000	0.000	0.000	0.000	0.000	0.000
12	1	0.000	0.000	0.000	0.000	0.000	0.000	0.000	0.000	0.000
12	2	0.000	0.000	0.000	0.000	0.000	0.000	0.000	0.000	0.000
12	3	0.000	0.000	0.000	0.000	0.000	0.000	0.000	0.000	0.000
12	4	0.000	0.000	0.000	0.000	0.000	0.000	0.000	0.000	0.000
12	5	0.000	0.000	0.000	0.000	0.000	0.000	0.000	0.000	0.000
12	6	0.000	0.000	0.000	0.000	0.000	0.000	0.000	0.000	0.000
12	7	0.000	0.000	0.000	0.000	0.000	0.000	0.000	0.000	0.000

12	8	0.000	0.000	0.000	0.000	0.000	0.000	0.000	0.000	0.000
12	9	0.000	0.000	0.000	0.000	0.000	0.000	0.000	0.000	0.000
12	10	0.000	0.000	0.000	0.000	0.000	0.000	0.000	0.000	0.000
12	11	0.000	0.000	0.000	0.000	0.000	0.000	0.000	0.000	0.000
12	12	0.000	0.000	0.000	0.000	0.000	0.000	0.000	0.000	0.000

[a] The CF parameters are only listed for non-negative values of q. The values with negative q are given by $B_{k-q} = (-1)^q B_{kq}^*$.

Table S9. Properties of the six lowest local quasi-doublets and one singlet of the Tb1 ions in **1** corresponding to the crystal-field split states in the local ground $^7F_6$ multiplets.

	E / cm^{-1}	g_x	g_y	g_z	θ [a]
Doublet 1	0.00, 0.10	0.000000	0.000000	17.968878	0.0°
Doublet 2	47, 48	0.000000	0.000000	14.916612	0.1°
Doublet 3	162, 166	0.000000	0.000000	11.770861	0.1°
Singlet	272, 302	0.000000	0.000000	8.611020	179.7°
Doublet 4	372				
Doublet 5	403, 433	0.000000	0.000000	14.648143	90.1°
Doublet 6	498, 502	0.000000	0.000000	17.489098	90.8°

[a] The angle between the principal magnetic axis of the given doublet and the that of the ground doublet.

Table S10. Properties of the six lowest local quasi-doublets and one singlet of the Tb2 ions in **1** corresponding to the crystal-field split states in the local ground $^7F_6$ multiplets.

	E / cm^{-1}	g_x	g_y	g_z	θ [a]
Doublet 1	0.00, 0.05	0.000000	0.000000	17.959387	0.0°
Doublet 2	78, 79	0.000000	0.000000	15.044064	8.6°
Doublet 3	199, 203	0.000000	0.000000	11.811699	5.7°
Singlet	304, 349	0.000000	0.000000	8.872564	176.9°
Doublet 4	408				
Doublet 5	436, 463	0.000000	0.000000	14.104493	90.0°
Doublet 6	515, 518	0.000000	0.000000	16.413457	89.5°

[a] The angle between the principal magnetic axis of the given doublet and the that of the ground doublet.

5. Magnetic Circular Dichroism (MCD) spectra

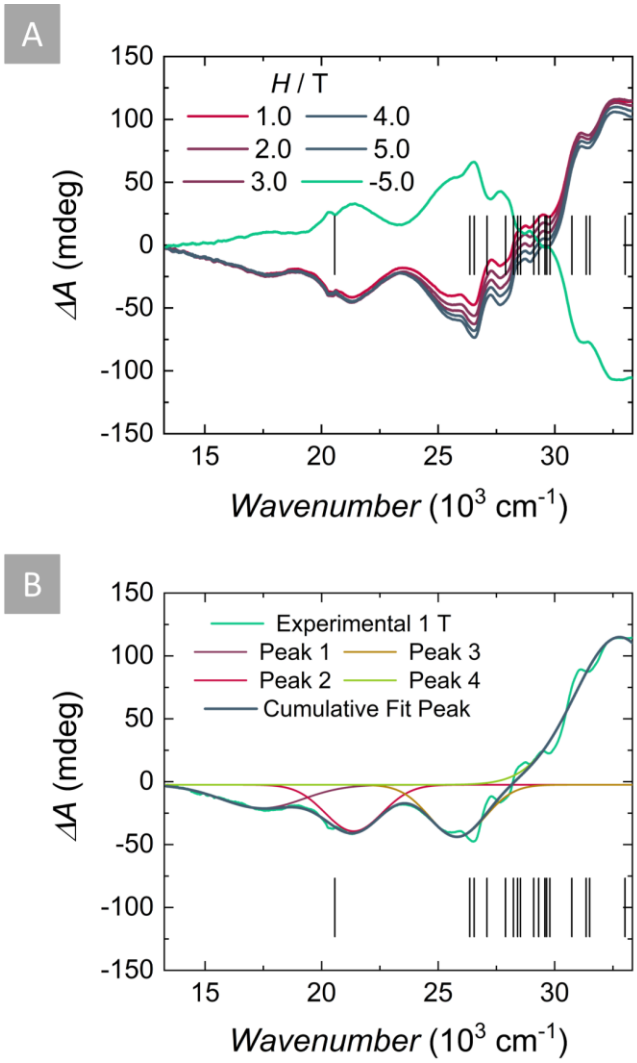

Fig. S16: (A) MCD spectra obtained at 1.9 K at different applied magnetic fields in wavenumber scale. (B) Deconvolution of the MCD spectrum obtained at 1.9 K with an applied field of 1 T. The broad band was deconvoluted in four different components related to the ligand absorptions. Black vertical lines in (A) and (B) indicate the position of Tb^{III} excited states, according to Carnall[26] (Table S11) and agrees with the sharp peaks and dips overlapping the ligand broad bands.

Table S11. Tb^{III} excited energy levels according to Carnall.[26]

Energy / cm^{-1}	$^{2S+1}L_J$ label
20568	$^5D_4$
26360	$^5D_3$
26547	$^5G_6$
27095	$^5L_{10}$
27891	$^5G_5$
28231	$^5D_2$
28411	$^5G_4$
28532	$^5L_9$
29101	$^5G_3$
29314	$^5L_8$
29581	$^5L_7$
29655	$^5G_2$
29794	$^5L_6$
30734	$^5D_1$
31348	$^5D_0$
31503	$^5H_7$
33015	$^5H_6$

6. References

[1] K. V. Domasevitch, I. A. Gural′skiy, P. V. Solntsev, E. B. Rusanov, H. Krautscheid, J. A. K. Howard, A. N. Chernega, *Dalton Trans.*, **2007**, 3140–3148.
[2] S. Demir, J. M. Zadrozny, M. Nippe, J. R. Long, *J. Am. Chem. Soc.*, **2012**, *134*, 18546–18549.
[3] G. M. Sheldrick, SADABS, *Bruker/Siemens Area Detector Absorption Correction Program V.2.0.3*, Bruker AXS: Madison, WI, 2003.
[4] G. M. Sheldrick, *Acta Cryst*, **2015**, *A71*, 3–8.
[5] G. M. Sheldrick, *Acta Cryst*, **2015**, *C71*, 3–8.
[6] N. Mavragani, A. A. Kitos, A. Mansikkamäki, M. Murugesu, *Inorg. Chem. Front.*, **2022**, *10*, 259–266.
[7] F. Bertinotti, C. Giacomello, A. M. Liquori, *Acta Cryst*, **1956**, *9*, 510–514.
[8] D. Reta, N. F. Chilton, *Phys. Chem. Chem. Phys.*, **2019**, *21*, 23567-23575.
[9] Gaussian 16, Revision C.01, M. J. Frisch, G. W. Trucks, H. B. Schlegel, G. E. Scuseria, M. A. Robb, J. R. Cheeseman, G. Scalmani, V. Barone, G. A. Petersson, H. Nakatsuji, X. Li, M. Caricato, A. V. Marenich, J. Bloino, B. G. Janesko, R. Gomperts, B. Mennucci, H. P. Hratchian, J. V. Ortiz, A. F. Izmaylov, J. L. Sonnenberg, D. Williams-Young, F. Ding, F. Lipparini, F. Egidi, J. Goings, B. Peng, A. Petrone, T. Henderson, D. Ranasinghe, V. G. Zakrzewski, J. Gao, N. Rega, G. Zheng, W. Liang, M. Hada, M. Ehara, K. Toyota, R. Fukuda, J. Hasegawa, M. Ishida, T. Nakajima, Y. Honda, O. Kitao, H. Nakai, T. Vreven, K. Throssell, J. A. Montgomery, Jr., J. E. Peralta, F. Ogliaro, M. J. Bearpark, J. J. Heyd, E. N. Brothers, K. N. Kudin, V. N. Staroverov, T. A. Keith, R. Kobayashi, J. Normand, K. Raghavachari, A. P. Rendell, J. C. Burant, S. S. Iyengar, J. Tomasi, M. Cossi, J. M. Millam, M. Klene, C. Adamo, R. Cammi, J. W. Ochterski, R. L. Martin, K. Morokuma, O. Farkas, J. B. Foresman, and D. J. Fox, *Gaussian, Inc.*, Wallingford CT, **2016**.
[10] a) J. P. Perdew, K. Burke, M. Ernzerhof. *Phys. Rev. Lett.*, **1996**, *77*, 3865–3868; b) J. P. Perdew, K. Burke, M. Ernzerhof. *Phys. Rev. Lett.*, **1996**, *78*, 1396.
[11] a) M. Dolg, H. Stoll, A. Savin, H. Preuß. *Theor. Chim. Acta.* **1989**, *75*, 173–194; b) D. Andrae, U. Häußermann, M. Dolg, H. Stoll, H. Preuß. *Theor. Chim. Acta.* **1990**, *77*, 123–141.
[12] F. Weigend, R. Ahlrichs. *Phys. Chem. Chem. Phys.* **2005**, *7*, 3297–3305.
[13] N. Mavragani, D. Errulat, D. A. Gálico, A. A. Kitos, A. Mansikkamäki, M. Murugesu. *Angew. Chem. Int. Ed.* **2021**, *60*, 24206–24213.
[14] L. Ungur, L. F. Chibotaru. *Chem. Eur. J.* **2017**, *23*, 3708–3718.
[15] a) B. O. Roos in *Advances in Chemical Physics*, *Ab Initio Methods in Quantum Chemistry II*, Vol. 69 (Ed.: K. P. Lawley), Wiley, New York, **1987**, pp. 399–455; b) P. Siegbahn, A. Heiberg, B. Roos, B. Levy. *Phys. Scripta*, **1980**, *21*, 323–327; c) B. O. Roos, P. R. Taylor, P. E. M. Siegbahn. *Chem. Phys.*, **1980**, *48*, 157–173; d) P. E. M. Siegbahn, J. Almlöf, A. Heiberg, B. Roos. *J. Chem. Phys.*, **1981**, *74*, 2384–2396; e) B. O. Roos, R. Lindh, P. Å. Malmqvist, V. Veryazov, P.-O. Widmark. *Multiconfigurational Quantum Chemistry.* Wiley, Hoboken, NJ, **2016**.
[16] a) F. Neese. *WIREs Comput. Mol. Sci.* **2017**, *8*, e1327; b) F. Neese, F. Wennmohs, U. Becker, C. Riplinger. *J. Chem. Phys.* **2020**, *152*, 224108; c) F. Neese. *J. Comp. Chem.* **2022**, *44*, 381–396.
[17] a) C. Angeli, R. Cimiraglia, S. Evangelisti, T. Leininger, J.-P. Malrieu. *J. Chem. Phys.* **2001**, *114*, 10252–10264; b) C. Angeli, R. Cimiraglia, J.-P. Malrieu. *Chem. Phys. Lett.* **2001**, *350*, 297–305; c) C. Angeli, R. Cimiraglia, J.-P. Malrieu. *J. Chem. Phys.* **2002**, *117*, 9138–9153.
[18] a) M. Douglas, N. M. Kroll. *Ann. Phys.* **1974**, *82*, 89–155; b) B. A. Heß. *Phys. Rev. A.* **1986**, *33*, 3742–3748.
[19] a) F. Neese, T. Petrenko, D. Ganyushin, G. Olbrich. *Coord. Chem. Rev.* **2007**, *251*, 288–327; b) M. Atanasov, D. Aravena, E. Suturina, E. Bill, D. Maganas, F. Neese. *Coord. Chem. Rev.* **2015**, *289–290*, 177–214.

[20] a) F. Neese. *J. Chem. Phys.* **2005**, *122*, 034107; b) A. Berning, M. Shcweizer, H.-J. Werne, P. J. Knowles, P. Palmieri. *Mol. Phys.* **2000**, *98*, 1823–1833; c) B. A. Heß, C. M. Marian, U. W. Wahlgren, O. Gropen. *Chem. Phys. Lett.* **1996**, *251*, 365–371.
[21] D. A. Pantazis, F. Neese. *J. Chem. Theory Comput.* **2009**, *5*, 2229–2238.
[22] D. A. Pantazis, X.-Y. Chen, C. R. Landis, F. Neese. *J. Chem. Theory Comput.* **2008**, *4*, 908–919.
[23] G. L. Stoychev, A. A. Auer, F. Neese. *J. Chem. Theory Comput.* **2017**, *13*, 554–562.
[24] L. F. Chibotaru, L. Ungur. *J. Chem. Phys.*, **2012**, *137*, 064112.
[25] a) N. Iwahara, L. F. Chibotaru. *Phys. Rev. B.* **2015**, *91*, 174438; b) N. Iwahara, L. Ungur, L. F. Chibotaru. *Phys. Rev. B.*, **2018**, *98*, 054436.
[26] W. T. Carnall, H. Crosswhite and H. M. Crosswhite, *Energy level structure and transition probabilities in the spectra of the trivalent lanthanides in LaF_3*, U.S. Department of Energy-Office of Scientific and Technical Information, United states: N. p., 1978.